Tightly Coupled INS/GPS with Bias Estimation for UAV Applications

Michael George, Salah Sukkarieh
Centre for Autonomous Systems
University of Sydney, Australia
{m.george, salah}@cas.usyd.edu.au

Abstract

This paper presents an analysis of a proposed tightly coupled Inertial/GPS navigation system for UAV applications. An indirect, error state extended Kalman filter is employed to estimate vehicle position, velocity, attitude and IMU bias errors. The indirect configuration linearises the state transition matrix and greatly reduces the required feedback frequency. Standard GPS C/A code pseudo-ranges are used directly to update the Kalman filter. The advantage of this configuration arises in situations of poor GPS availability. Traditional loosely coupled filters can deliver no new information to the filter when the observed satellite number falls below four. In the tightly coupled configuration, all available information is delivered to the filter even in situations where only one satellite remains observable. The extension of the vehicle states to include IMU biases further improves navigation accuracy by constraining drift during the INS alone cycle and in periods of low GPS observability. Both algorithms are suited to a low cost implementation. Results from flight trials of the Brumby Mk. III UAV are presented.

1 Introduction

Inertial Measurement Units (IMUs) provide high frequency acceleration and rotation rate data that can be used independent of vehicle models. The equations of inertial navigation are essentially integrators meaning inherent noise and biases in the system lead to unbounded, exponential error growth in time. The desirability of aiding inertial sensors with GPS measurements has long been known [Titterton, Weston, 2004].

The traditional approach to INS/GPS integration with Kalman filters leads to a configuration termed 'loosely coupled'. In this structure a GPS filter (generally EKF or Least-squares recursion) processes the GPS signals and outputs three dimensional position (and possibly velocity) in the standard GPS Earth Centred Earth Fixed (ECEF) reference frame. The design of the GPS system requires four satellites to be tracked in order to solve for three dimensional position (a fourth time uncertainty is also solved). When less than four satellites are visible, stand-alone three dimensional GPS positioning cannot be accomplished. Loosely coupled configurations employ a second, master Kalman Filter to predict inertial sensor errors from the equations of inertial navigation. The filter is updated with direct observations of the position error formed from the outputs of the inertial unit and the GPS filter. The standard Kalman filter equations are optimal when sensor observations are unbiased with white noise. By filtering the GPS data twice this optimality constraint is effectively abandoned.

Tightly coupled Kalman filtering for INS/GPS integration is not a new innovation in itself but it has found use in the autonomous vehicle community rarely and only recently [Wendel, Trommer, 2004]. GPS ranging signals are fused directly in the update stage of the Kalman filter. The more satellites used in the ranging process the more information the filter has to constrain the inertial navigation solution. In a situation of degraded GPS availability however a tightly coupled configuration is capable of updating the filter with only one visible satellite. In addition, a tightly coupled filter processes the GPS signals directly. In a well designed system this increases the chance of optimal filter performance.

GPS availability is a function of many variables. In ground vehicle applications the primary degradation occurs from signal shading as the vehicle traverses close to natural features or buildings. In UAV applications this situation is unlikely to occur, however in dynamic

situations, the UAV's wings can shade satellite signals. This is a situation that has occurred in the autonomous UAV literature, [Kim, Sukkarieh, 2003]. In addition GPS signals are readily degraded by deliberate means.

2 Navigation Algorithms

2.1 Equations of Inertial Navigation

The standard equations of inertial navigation are implemented in a high frequency (100Hz) loop, external to the Kalman filter. A local level North, East, Down (NED) coordinate system is chosen as appropriate to the short range applications we are considering but could readily be extended to a global frame without loss of generality. From [Titterton, Weston, 2004]

$$\dot{\mathbf{v}}^e = \mathbf{C}_{\mathbf{b}}^{\mathbf{e}}\mathbf{f}^{\mathbf{b}} - 2\omega_{\mathbf{ie}}^{\mathbf{e}} \times \mathbf{v}^{\mathbf{e}} + \mathbf{g}_{\mathbf{l}}^{\mathbf{e}} \tag{1}$$

Where:

- $\mathbf{v}^{\mathbf{e}}$ $[3 \times 1]$ components of the vehicle velocity
- $\mathbf{C}_{\mathbf{b}}^{\mathbf{e}}$ Direction cosine matrix relating body (IMU) frame to NED frame
- $\omega_{\mathbf{ie}}^{\mathbf{e}}$ $[3 \times 1]$ Components of earth rotation vector
- $\mathbf{f}^{\mathbf{b}}$ $[3 \times 1]$ Specific force vector from accelerometers in body (IMU) frame
- $\mathbf{g}_{\mathbf{l}}^{\mathbf{e}}$ Local gravity vector (including centripetal effects)
- $\mathbf{n}^{\mathbf{e}}$ Arbitrary vector $\mathbf{n}$ written in NED frame

Equation (1) is solved via a first order discretisation and double euler integration to give vehicle velocity and position

$$\mathbf{v}^{\mathbf{e}}(k+1) = \mathbf{v}^{\mathbf{e}}(k) + \dot{\mathbf{v}}^{\mathbf{e}}(k)\Delta t \tag{2}$$

$$\mathbf{P}^{\mathbf{e}}(k+1) = \mathbf{P}^{\mathbf{e}}(k) + \mathbf{v}^{\mathbf{e}}(k)\Delta t \tag{3}$$

Equations (2) and (3) provide vehicle translations in the NED coordinate system. Vehicle orientation needs to be tracked in order to accomplish the transformation, $\mathbf{C}_{\mathbf{b}}^{\mathbf{e}}$, of inertial measurements in the body fixed coordinates to the NED coordinates. In this work, the rotation components of vehicle motion are defined by Euler angles, representing roll, pitch and yaw respectively, [Titterton, Weston, 2004].

$$\begin{bmatrix} \dot{\phi} \\ \dot{\theta} \\ \dot{\psi} \end{bmatrix} = \begin{bmatrix} 1 & \frac{s_\phi s_\theta}{c_\theta} & \frac{c_\phi s_\theta}{c_\theta} \\ 0 & c_\phi & -s_\phi \\ 0 & \frac{s_\phi}{c_\theta} & \frac{c_\phi}{c_\theta} \end{bmatrix} \begin{bmatrix} \omega_x \\ \omega_y \\ \omega_z \end{bmatrix} \tag{4}$$

Denoting the three Euler angles by the vector $\mathbf{\Psi}$, equation (4) is discretised to first order and solved via Euler integration.

$$\mathbf{\Psi}(k+1) = \mathbf{\Psi}(k) + \dot{\mathbf{\Psi}}(k)\Delta t \tag{5}$$

The direction cosine matrix from equation (1) is then constructed directly from the Euler angles.

$$\mathbf{C}_{\mathbf{b}}^{\mathbf{e}} = \begin{bmatrix} c_\theta c_\psi & -c_\phi s_\psi + s_\phi s_\theta c_\psi & s_\phi s_\psi + c_\phi s_\theta c_\psi \\ c_\theta s_\psi & c_\phi c_\psi + s_\phi s_\theta s_\psi & -s_\phi c_\psi + c_\phi s_\theta s_\psi \\ -s_\theta & s_\phi c_\theta & c_\phi c_\theta \end{bmatrix} \tag{6}$$

where $s_{\mathbf{\Psi}_i}$ and $c_{\mathbf{\Psi}_i}$ are shorthand notations for $\sin \mathbf{\Psi}_i$ and $\cos \mathbf{\Psi}_i$ respectively. The propagation of the direction cosine matrix will also be useful for further derivations and is given by [Savage, 2000]

$$\dot{\mathbf{C}}_{\mathbf{b}}^{\mathbf{e}} = \mathbf{C}_{\mathbf{b}}^{\mathbf{e}}[\omega_{\mathbf{ib}}^{\mathbf{b}}\times] - [\omega_{\mathbf{ie}}^{\mathbf{e}}\times]\mathbf{C}_{\mathbf{b}}^{\mathbf{e}} \tag{7}$$

Where:

- $\omega_{\mathbf{ib}}^{\mathbf{b}}$ $[3 \times 1]$ Components of body rotation vector written in body frame (IMU measurements)
- $\omega_{\mathbf{ie}}^{\mathbf{e}}$ $[3 \times 1]$ Components of earth rotation vector written in NED frame
- $[\mathbf{n}\times]$ Skew symmetric matrix notation for arbitrary vector $\mathbf{n}$

2.2 Equations of GPS Navigation

The structure of GPS signals are specified in [Author Unknown, 1995]. In this work, the standard, non-differential, civilian signal is used. This represents the lowest standard of accuracy but requires no other external infrastructure and is the lowest cost GPS solution available. The standard measurement of the GPS system is the pseudo-range. This defines the approximate range from the user GPS receiver antenna to a particular satellite. The pseudo-range is the true geometric range corrupted with errors and with a minimal set of error corrections can be specified by

$$\rho_j = r_j + \delta\rho_{r,clk} + \delta\rho_{ion} - \delta\rho_{s,clk} + v \tag{8}$$

Where:

- ρ_j Pseudo-range from the user to the j^{th} satellite
- r_j Geometric range from the user to the j^{th} satellite
- $\delta\rho_{r,clk}$ Range equivalent receiver clock bias offset from GPS system time
- $\delta\rho_{s,clk}$ Range equivalent satellite clock bias offset from GPS system time
- $\delta\rho_{ion}$ Ionospheric signal attenuation error
- v Zero mean white noise

Satellite position is determined from broadcast ephemeris parameters. Included in this broadcast is a correction for the satellite clock bias. There are a number of established models that account for atmospheric perturbations of the signal. In this work the

Klobuchar Ionospheric model [Rizos, 1995] is used. This model is fully defined by eight coefficients broadcast as part of the standard GPS signal.

$$\delta\rho_{ion} = 5 \times 10^{-9} + A\cos\frac{2\pi(t-t_0)}{P} \tag{9}$$

Where A and P represent the broadcast Klobuchar co-efficients summed with the latitude of the ionospheric sub-point and t_0 represents the time of day (usually midday) at which ionospheric attenuation is greatest.

Once compensation for satellite clock bias and atmospheric effects are applied equation (8) is reduced to

$$\rho_j = r_j + \delta\rho_{r,clk} + v \tag{10}$$

Equation (10) is then simultaneously solved for position and user clock bias resulting in the desired navigation solution. The geometric range from equation (10) can be expanded explicitly

$$\rho_j = \left[(X_j - x)^2 + (Y_j - y)^2 + (Z_j - z)^2\right]^{\frac{1}{2}} + \delta\rho_{r,clk} + v \tag{11}$$

Where:

$[X_j, Y_j, Z_j]^T$	$[3 \times 1]$ Components of the j^{th} satellite's position in ECEF coordinates
$[x, y, z]^T$	$[3 \times 1]$ Components of user's filtered position in ECEF coordinates

A transformation from NED to ECEF and vice versa is required for the calculation of Equation (11). These transformations are complicated by an ellipsoidal earth model with large GPS satellite altitudes. A number of closed form and iterative solutions exist and the reader who is interested is directed to [Bomford, 1971].

3 Kalman Filter Structure

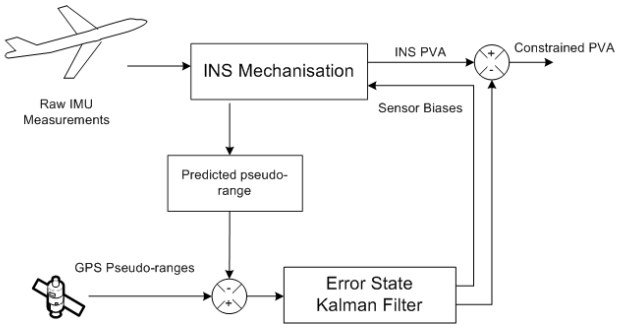

Figure 1: Indirect Tightly Coupled Kalman Filter.

This work uses an indirect error state model for inertial navigation systems. A schematic of the cycle is shown in Figure (1). The equations are mechanised in a local level, North, East, Down coordinate system with a flat earth assumption. The error state vector is defined to include position and velocity errors, attitude misalignments, user clock bias error and inertial sensor bias errors.

$$\mathbf{x} = \begin{bmatrix} \delta\mathbf{P_e} \\ \delta\mathbf{v_e} \\ \delta\mathbf{\Phi} \\ \delta c_b \\ \delta\mathbf{f^b} \\ \delta\omega^{\mathbf{b}}_{\mathbf{ib}} \end{bmatrix} \tag{12}$$

Where:

$\delta\mathbf{P^e}$	$[3 \times 1]$ Error components of the inertial calculated position
$\delta\mathbf{v^e}$	$[3 \times 1]$ Error components of the inertial calculated velocity
$\delta\mathbf{\Phi}$	$[3 \times 1]$ Misalignment errors that affect the transformation $\mathbf{C^e_b}$
δc_b	$[1 \times 1]$ Error in the predicted user clock bias (in units of range)
$\delta\mathbf{f^b}$	$[3 \times 1]$ Error components of the accelerometer biases
$\delta\omega^{\mathbf{b}}_{\mathbf{ib}}$	$[3 \times 1]$ Error components of the gyroscope biases

3.1 Inertial Error Model

In state notation the inertial navigation error equations propagate as a linear, time-variant first order system driven by white noise

$$\dot{\mathbf{x}}_{ins} = \mathbf{F}_{ins}\mathbf{x}_{ins} + \mathbf{G}_{ins}\mathbf{w}_{ins} \tag{13}$$

The input driving noise, $\mathbf{w}_{ins}$ is defined as a vector of three accelerometer components and three gyroscope components.

$$\mathbf{w} = \begin{bmatrix} \mathbf{w_{f^b}} \\ \mathbf{w}_{\omega^{\mathbf{b}}_{\mathbf{ib}}} \end{bmatrix} \tag{14}$$

The first component $\mathbf{w_{f^b}}$ represents the remaining (white) noise on the accelerometers in the body frame (to which the IMU is fixed) after the biases are removed and the second component $\mathbf{w}_{\omega^{\mathbf{b}}_{\mathbf{ib}}}$ is the remaining (white) noise on the gyroscopes measuring rotation rates of the body frame relative to inertial space, written in the body frame, after biases are removed. The input noise $\mathbf{w}$ is characterised by variance $\mathbf{Q}$.

The system and noise input matrices, representing the linear dynamics of the inertial system errors are derived by perturbing equations (1) and (7). The derivation of equations describing the propagation of the biases is left until the next section. The inertial error equations will be presented here without a

derivation which can be found in [Titterton, Weston, 2004]. In continuous time the components of Equation (13), representing the inertial position, velocity and misalignments from Equation (12) are

$$\mathbf{F}_{ins} = \begin{bmatrix} \mathbf{0} & \mathbf{I} & \mathbf{0} \\ \mathbf{0} & [-2\omega^{\mathbf{e}}_{\mathbf{ie}}\times] & [(\mathbf{C}^{\mathbf{e}}_{\mathbf{b}}\mathbf{f}^{\mathbf{b}})\times] \\ \mathbf{0} & \mathbf{0} & [-\omega^{\mathbf{e}}_{\mathbf{ie}}\times] \end{bmatrix} \quad (15)$$

$$\mathbf{G}_{ins} = \begin{bmatrix} \mathbf{0} & \mathbf{0} \\ \mathbf{C}^{\mathbf{e}}_{\mathbf{b}} & \mathbf{0} \\ \mathbf{0} & -\mathbf{C}^{\mathbf{e}}_{\mathbf{b}} \end{bmatrix} \quad (16)$$

Where the components of $\mathbf{F}_{ins}$ and $\mathbf{G}_{ins}$ are

$\mathbf{0}$	Appropriately sized zero matrix
$\mathbf{I}$	Appropriately sized identity matrix
$\omega^{\mathbf{e}}_{\mathbf{ie}}$	$[3 \times 1]$ earth rotation vector written in NED frame
$\mathbf{C}^{\mathbf{e}}_{\mathbf{b}}$	Direction cosine matrix relating body and NED frame
$\mathbf{f}^{\mathbf{b}}$	$[3 \times 1]$ specific force vector from accelerometers
$[\mathbf{n}\times]$	Skew symmetric matrix notation for arbitrary vector $\mathbf{n}$

3.2 Bias Error Model

In this section both clock bias and inertial sensor biases are considered together. Clock bias is an essential part of the GPS solution and cannot be omitted. Inertial bias estimation has the potential to improve navigation solutions in two ways. It smoothes the trajectory in normal operation by reducing the drift in the INS integrations and it improves robustness and recoverability by greatly reducing the drift experienced in failed or denied GPS environments.

The bias errors are estimated as Brownian processes. In discrete time this is

$$\delta c_b(k+1) = c_b(k) + w_c \quad (17)$$

$$\delta\mathbf{f}^{\mathbf{b}}(k+1) = \delta\mathbf{f}^{\mathbf{b}}(k) + \mathbf{w}_{\mathbf{accel}} \quad (18)$$

$$\delta\omega^{\mathbf{b}}_{\mathbf{ib}}(k+1) = \delta\omega^{\mathbf{b}}_{\mathbf{ib}}(k) + \mathbf{w}_{\mathbf{gyro}} \quad (19)$$

We augment the inertial error state model

$$\mathbf{x} = [\mathbf{x}_{ins} \quad x_{clock\_bias} \quad \mathbf{x}_{ins\_biases}]^T \quad (20)$$

Here we have included accelerometer biases, $\delta\mathbf{f}^{\mathbf{b}}$ and gyroscope biases, $\delta\omega^{\mathbf{b}}_{\mathbf{ib}}$ into one term, $\mathbf{x}_{ins\_biases}$. The continuous state transition and noise input matrices from equations (15) and (16) are then extended

$$\mathbf{F} = \begin{bmatrix} \mathbf{F}_{ins} & \mathbf{0} & \mathbf{F}_{coupled} \\ \mathbf{0} & F_{clock\_bias} & \mathbf{0} \\ \mathbf{0} & \mathbf{0} & \mathbf{F}_{ins\_biases} \end{bmatrix} \quad (21)$$

$$\mathbf{G} = \begin{bmatrix} \mathbf{G}_{ins} & \mathbf{0} & \mathbf{0} \\ \mathbf{0} & G_{clock\_bias} & \mathbf{0} \\ \mathbf{0} & \mathbf{0} & \mathbf{G}_{ins\_biases} \end{bmatrix} \quad (22)$$

We can specify the elements in these matrices

$$\mathbf{F}_{coupled} = \begin{bmatrix} \mathbf{0} & \mathbf{0} \\ \mathbf{C}^{\mathbf{e}}_{\mathbf{b}} & \mathbf{0} \\ \mathbf{0} & -\mathbf{C}^{\mathbf{e}}_{\mathbf{b}} \end{bmatrix} \quad (23)$$

Equation (23) represents the way the INS biases (in body fixed coordinates) couple to the INS position, velocity and attitude error rates in the NED frame.

$$F_{clock\_bias} = [0] \quad (24)$$

Equation (24) represents the clock bias error transition as a random process in continuous time.

$$\mathbf{F}_{ins\_biases} = \begin{bmatrix} \mathbf{0} & \mathbf{0} \\ \mathbf{0} & \mathbf{0} \end{bmatrix} \quad (25)$$

Equation (25) is analogous to equation (24) and represents the random INS bias error modeling in continuous time.

$$G_{clock\_bias} = 1 \quad (26)$$

$$\mathbf{G}_{ins\_biases} = \mathbf{I} \quad (27)$$

Equations (26) and (27) imply direct transmission of bias noises into the bias error state.

3.3 Kalman Filter Prediction

The indirect structure depicted in Figure (1) feeds back the estimated errors after each update cycle of the filter. This feedback represents the entire knowledge of the errors in the state and hence resets the state mean to zero. The prediction cycle then involves a prediction of covariance only. Given a suitably initialised covariance matrix, $\mathbf{P}(k_0|k_0)$, and a discretisation (omitted for brevity) we have

$$\mathbf{P}(k+1|k) = \mathbf{F}\mathbf{P}(k|k)\mathbf{F}^T + \mathbf{Q} \quad (28)$$

3.4 Kalman Filter Observation

The linear Kalman filter observation takes the form:

$$\mathbf{z} = \mathbf{H}\mathbf{x} + \mathbf{v} \quad (29)$$

In this implementation, the available observations are non-linear pseudo-range errors, derived from the measured pseudo-range and a predicted pseudo-range based on the inertial calculated position

$$\delta\rho = \rho_{gps} - \rho_{pred,ins} \quad (30)$$

Where ρ_{gps} is the standard C/A code pseudo-range corrected for satellite clock bias and ionospheric attenuation

and $\rho_{pred,ins}$ is constructed from equation (11) via the INS position solution and clock bias estimate. The linear $\mathbf{H}$ matrix must link these pseudo-range errors to the relevant components of the state vector. In this work this is position and clock bias only. The first order Taylor series expansion of equation (11) is used.

$$\delta\rho = \frac{\partial \mathbf{h}}{\partial \mathbf{x}}\delta\mathbf{x} \quad (31)$$
$$= \mathbf{H}\delta\mathbf{x} \quad (32)$$

So for an arbitrary number of visible satellites $\mathbf{H}$ can be constructed

$$\mathbf{H} = \begin{bmatrix} \frac{\partial\rho_1}{\partial x} & \frac{\partial\rho_1}{\partial y} & \frac{\partial\rho_1}{\partial z} & \frac{\partial\rho_1}{\partial c_b} \\ \frac{\partial\rho_2}{\partial x} & \frac{\partial\rho_2}{\partial y} & \frac{\partial\rho_2}{\partial z} & \frac{\partial\rho_2}{\partial c_b} \\ & \cdots & & \\ \frac{\partial\rho_n}{\partial x} & \frac{\partial\rho_n}{\partial y} & \frac{\partial\rho_n}{\partial z} & \frac{\partial\rho_n}{\partial c_b} \end{bmatrix} \quad (33)$$

For brevity we have included only the non-zero terms in $\mathbf{H}$ and omitted the extra dimensions corresponding to zeros. The elements of $\mathbf{H}$ consist of:

$$\frac{\partial\rho_j}{\partial x} = \frac{-(X_j - x)}{[(X_j - x)^2 + (Y_j - y)^2 + (Z_j - z)^2]^{\frac{1}{2}}}$$
$$\frac{\partial\rho_j}{\partial y} = \frac{-(Y_j - y)}{[(X_j - x)^2 + (Y_j - y)^2 + (Z_j - z)^2]^{\frac{1}{2}}}$$
$$\frac{\partial\rho_j}{\partial z} = \frac{-(Z_j - z)}{[(X_j - x)^2 + (Y_j - y)^2 + (Z_j - z)^2]^{\frac{1}{2}}}$$
$$\frac{\partial\rho_j}{\partial c_b} = 1 \quad (34)$$

The state and covariance updates are performed in the typical fashion.

4 Analysis Procedure

The Kalman filter structure described in the preceding sections was implemented with post-processed raw INS and GPS measurements. The data was collected from the University of Sydney's Marulan test flight range in May, 2005. A Brumby Mk. III UAV was flown through a mission scenario consisting of pre-defined paths designed to bring vision sensors into locations in which ground targets could be observed. The primary path components consist of straight line trajectories, figure eights and constant radius orbits.

Shading of GPS signals by the wing has been a common occurrence in Brumby missions to date. In such situations, navigation accuracy has been severely degraded especially in the altitude axis [Kim, Sukkarieh, 2003]. To evaluate bias estimation a comparison of a stationary period after landing with and without bias estimation is presented. This represents a period where bias estimates have converged and where the vehicle dynamics will not cloud the analysis. A comparison of vehicle drift in a period of GPS outage with and without bias estimation is also presented.

5 Results

Figure (2) presents a plan view of part of the flight trajectory. A simulated GPS outage occurs for 20 seconds during a smooth, slow turn. A tightly coupled solution with full satellite availability is used as a baseline solution for comparison. Results from a tightly coupled solution with one, two, three satellites are compared to a loosely coupled solution without GPS aiding (as will occur with any number of satellites below four). Figure (3) expands the image at the end of the period of reduced GPS observability for clarification. Figure (4) shows results from the altitude axis for the same situation.

Figures (2), (3) and (4) demonstrate the possible improvements in navigation accuracy and reliability that can be obtained with the tightly coupled configuration. The altitude axis is consistently the worst case. In this axis results show that for two or three visible satellites positioning errors are reduced by a factor of approximately 5. For one visible satellite positioning errors are improved by an approximate factor of 1.5.

Figures (5) and (6) present the raw accelerometer and gyro measurements with and without bias correction. Bias estimation is correcting the raw measurements. The presence of undesirable harmonics in two of the corrected gyroscope measurements is due to filter tuning and will be further examined in later work.

Figure (7) demonstrates the improvement in INS alone drift that can be achieved with bias estimation. In a simulated, partial GPS outage lasting 20 seconds, position error in the horizontal axes was improved by a factor of 15 where only two GPS satellites were visible.

6 Future Considerations

Future work will include a more extensive, statistical analysis of the errors in position, velocity and attitude. Vision observations of known map landmarks will be incorporated with the goal of utilising all available information for localisation and navigation in the most robust and autonomous manner possible.

7 Conclusion

This paper has presented an overview of potential enhancements that can be made to current low, cost UAV

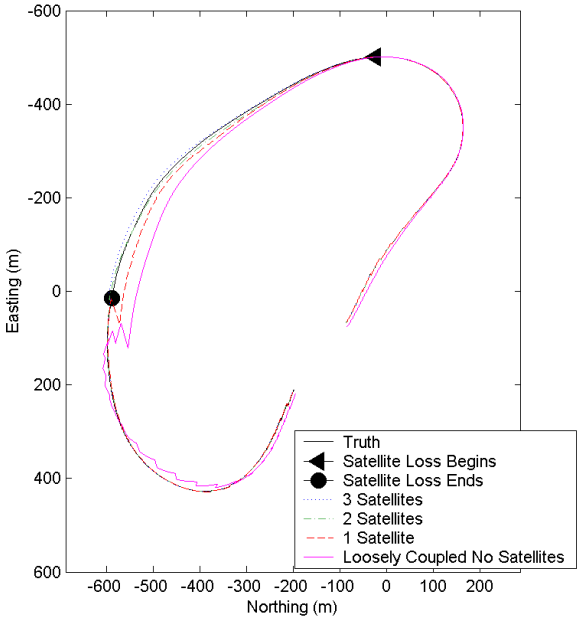

Figure 2: Comparison of horizontal position errors after simulated GPS satellite loss of 20s. Reducing numbers of visible satellites compared with baseline and loosely coupled solutions demonstrate significant improvements in error magnitude.

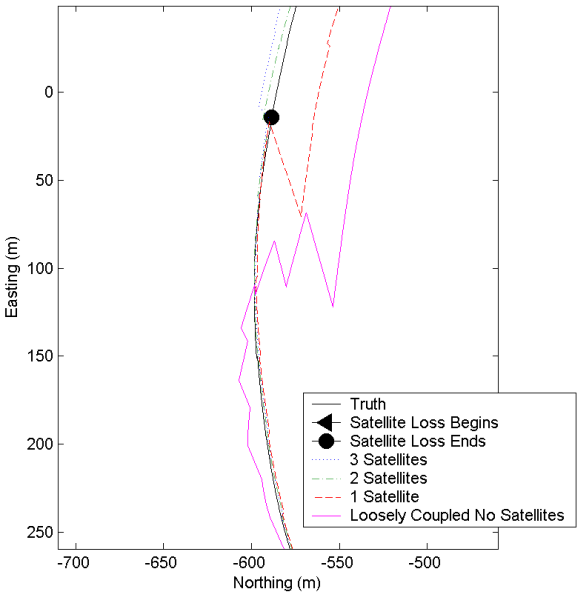

Figure 3: Comparison of horizontal errors after simulated GPS satellite loss - magnified.

navigation systems. Results were presented based on the current configuration of the Brumby UAV. The work has focussed on altering the INS/GPS integration structure and extending the estimation process to include biases in the inertial navigation sensors. Motivating the work was the improvement to be gained by restructuring sensor measurements that are already available.

References

[Author Unknown, 1995] Author Unknown *Global Positioning System Standard Positioning Service Signal Specification 2nd Ed.*. United States Coastguard Navigation Center. 1995. Available online. *http : //www.navcen.uscg.gov/pubs/gps/sigspec/gpsspsa.pdf*

[Bomford, 1971] G. Bomford. *Geodesy*. Clarendon Press. Oxford. 1971.

[Godha, 2004] S. Godha. *Strategies for GPS/INS Integration*. University of Calgary, ENGO 623 Course Lecture Notes. Available online. 2004.

[Grewal *et al.*, 2001] M. Grewal, L. Weill, A. Andrews. *Global Positioning Systems, Inertial Navigation and Integration*. John Wiley and Sons. New York. 2001.

[Kim, Sukkarieh, 2003] JH Kim. , S. Sukkarieh. *A baro-altimeter augmented INS/GPS navigation system for an uninhabited aerial vehicle*. The 6th International Conference on Satellite Navigation Technology (SATNAV 03) 23-25 July, Australia, Melbourne. July 23, 2003.

[Minkler *et al.*, 1990] G. Minkler and J. Minkler. *Aerospace Coordinate Systems and Transformations*. Magellan. Baltimore. 1990.

[Pitman, 1962] G. Pitman Jr. *Inertial Guidance*. University of California Engineering and Physical Science Extension Series. Wiley Interscience. New York. 1962.

[Rizos, 1995] C. Rizos. *Principles and Practice of GPS Surveying*. Version 1.1, UNSW, 1999. Available Online. *http : //www.gmat.unsw.edu.au/snap/*.

[Savage, 2000] P. Savage. *Strapdown Analytics Part 2*. Strapdown Associates. Maple Plain. 2000.

[Titterton, Weston, 2004] D.H. Titterton, J.L. Weston. *Strapdown Inertial Navigation Technology - 2nd Edition*. In IEE Radar, Sonar, Navigation and Avionics Series 17, N. Stewart, H. Griffiths, Eds. Institution of Electrical Engineers. Stevenage, UK. 2004.

[Wendel, Trommer, 2004] J. Wendel, G. Trommer. Tightly Coupled GPS/INS Integration for Missile Applications. Aerospace Science and Technology 8 (2004) pp. 627-634.

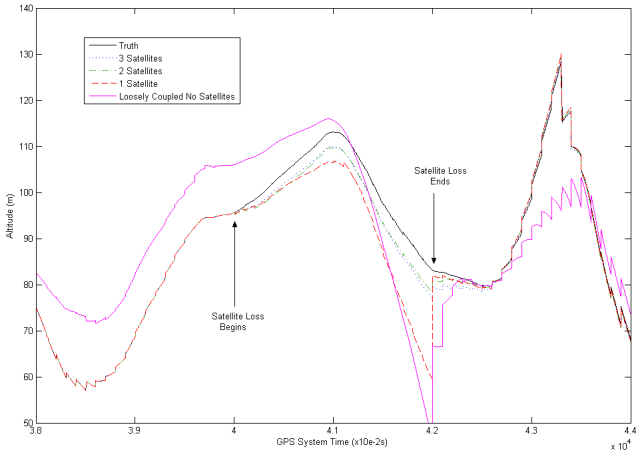

Figure 4: Comparison of vertical errors after simulated GPS satellite loss.

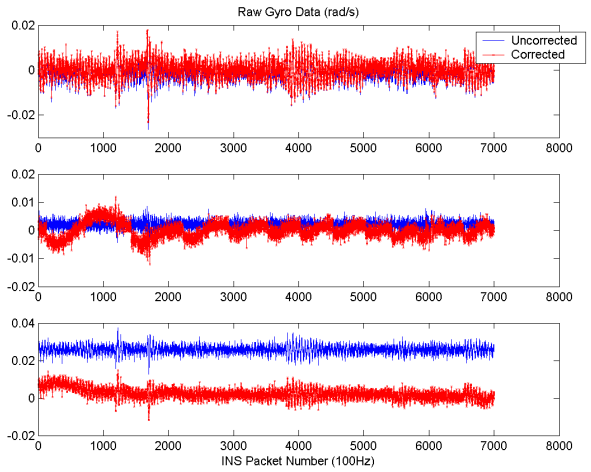

Figure 6: Gyroscope measurements with and without bias corrections taken from stationary period after landing.

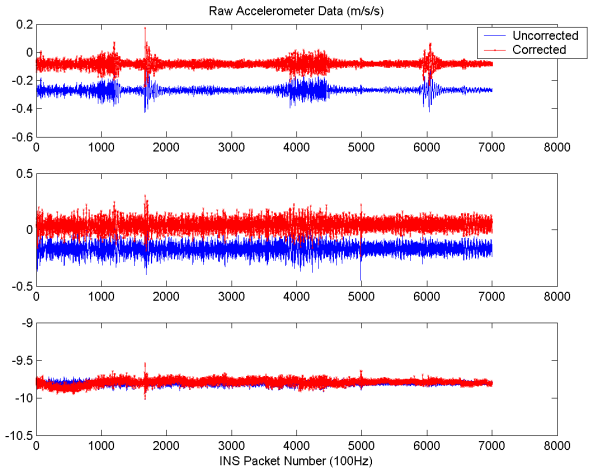

Figure 5: Accelerometer measurements with and without bias corrections taken from stationary period after landing.

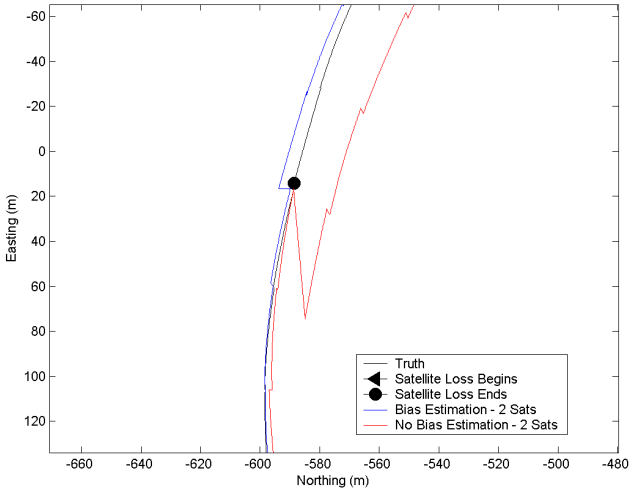

Figure 7: Comparison of horizontal position errors with and without bias estimation with two visible satellites. Unaided INS position is significantly improved by removing the biases - Magnified.